EXPERIMENTAL CHARACTERIZATION OF THE COMPRESSIVE BEHAVIOUR OF GRANITES

Vasconcelos, G.[1]; Lourenço, P. B.[2]

[1]Prof. Auxiliar, [2]Prof. Catedrático
ISISE, Instituto para a Sustentabilidade e Inovação em Engenharia Estrutural, University of Minho


RESUMO

This work intends to obtain the compressive mechanical properties and to improve the understanding of the fracture process of granites based on an enlarged experimental program of uniaxial compressive tests. It was possible to obtain the successful complete stress-strain diagrams, from which the elastic and fracture properties were derived, through an appropriate circumferential displacement control. A discussion on the parameters influencing the compressive behaviour is also performed.

1 - INTRODUÇÃO

Masonry is the oldest building material that survived until today, being used all over the world and is present in the most impressive historical structures. Conservation, rehabilitation and strengthening of the built heritage and protection of human lives are clear demands of modern societies and the evaluation of the stability conditions of the damaged ancient constructions involve frequently the usage of advanced numerical tools, where the knowledge of the mechanical properties of the stone masonry is required.

The pioneer work in the scope of fracture mechanics was carried out by Griffith (1920) (initially used to explain the differences found between the theoretical and experimental tensile strength of quasi-brittle materials), which postulated that quasi-brittle fracture initiated through tensile stress concentrations at the tips of small and thin cracks randomly distributed in the isotropic material. According to Lajtai et al. (1990), the Griffith theory or at least the basic assumption that fracture starts from flaws is fundamental to all investigations in quasi-brittle fracture. Several other studies have followed in order to obtain a better insight on the fracture of brittle materials regarding the mechanisms of crack initiation, crack inter-action, propagation and coalescence [Lajtai et al. (1990), Carpinteri et al. (1996)]. An issue commonly accepted in the fracture process under uniaxial compression is that nucleation, growth, interaction and coalescence of microcraks leads to macroscopic failure of rocks. Besides, in general, the fracture forming under uniaxial compression conditions, before attaining the peak load, is a tensile fracture. Therefore, the propagation of fracture occurs in the direction parallel to the maximum principal stress. It should be stressed that several experimental studies have been carried out recently in order to characterize the micro-cracking process of granites under compression [Eberhardt et al. (1999)]. Although some experimental studies have been carried out on strain localization detection in concrete and rocks [Vonk (1993)], and

apart from the extensive experimental characterization of concrete under multi-axial loading conditions carried out by Van Mier (1984), few information on the experimental characterization on the softening behaviour of rocks, namely granites, is available in literature. The obtainment of the complete stress-strain diagrams that comprise the ascending and the softening behaviour is practically non-existent in case of granites, namely high strength granites.

Thus, the main goal of the present research is the definition of the complete stress-strain diagrams of Portuguese granites. For this purpose, a campaign of uniaxial compression tests was carried out on selected granite lithotypes. For all granites, the characterization of the pre-peak fracture process is analyzed by means of the values of the crack initiation stress and the crack damage stress. Moreover, strain localization and softening characterization of granites are evaluated through the descending branch of post-peak diagrams. The factors that affect the compressive behaviour such as planar anisotropy (foliation and rift plane), weathering effects and moisture content are high-lighted. It should be stressed that the signify-cance of this study is the gathering of experimental data required as input data in advanced nonlinear numerical analysis of structural members of ancient structures where the granite plays the central role, together with full characterization of Portuguese lithotypes.

2 - EXPERIMENTAL TESTING

The granites adopted in the present work were mostly collected from the Northern region of Portugal. The selection of the granitic types was based on the mineralogical composition and grain size, aiming at providing a comprehensive sample of the Portuguese granites. In addition to these criteria, the presence of preferential orientation planes and weathering condition were also taken into account [Vasconcelos (2005)]. Due to this anisotropy, some granites were tested in two directions: parallel and perpendicular to the rift or foliation plans, see Table 1. The more weathered types of the same granite facies are distinguished with an asterisk (*).

Table 1:. Brief description of the selected granites.

Granite	Petrologic description	Loading directions
BA	Fine to medium-grained porphyritic biotite granite	// rift plane
GA, GA*	Fine to medium-grained, with porphyritic trend, two mica granite	// the rift plane
RM	Medium-grained biotite granite	// the rift plane
MC	Coarse-grained porphyritic biotite granite	// the rift plane
AF	Fine to medium-grained two mica granite	// and ⊥ foliation plane
MDB, MDB*	Fine to medium-grained two mica granite	// and ⊥ foliation plane
PTA, PTA*	Fine to medium-grained two mica granite	// and ⊥ foliation plane
PLA, PLA*	Medium to coarse-grained porphyritic biotite granite	// and ⊥ rift plane

2.1 -Specimens, test setup and test procedure

The specimens to be tested under uniaxial compression were prepared in accordance with ISRM suggested methods (1981) and ASTM D2938 (2002) standard. Following the recommendations, the test specimens shall be right circular cylinders having a height to diameter ratio between 2.0 and 3.0 and a diameter of not less than approximately 50mm. In addition, the diameter shall be at least 10 or 20 times the largest grain of the rock microstructure. The restriction for the height to diameter ratio is related to the influence of the boundary effects [Hudson and Harrison (1998)]. In spite of the size effects are not addressed here, it is important to refer that due to the limitations of the vertical loading actuator existing at the laboratory, a diameter of 75mm was adopted for all specimens. The length to diameter ratio was slightly higher than 2.0.

As the main goal of the present work is the characterization of the full compressive behaviour of all types of granites, uniaxial compression tests were carried out in a very

stiff frame connected with an appropriate closed-loop control system at the Structural Laboratory of University of Minho. Besides the equipment, the variable control is another central issue in the obtainment of complete stress-strain diagrams. The vertical displacement is not appropriate to obtain the softening behaviour of stiff rocks like granites as the axial strain does not increase monotonically and hence can not be used as feedback signal [Jansen et al. (1995)]. From the characteristic compressive behaviour of rocks or concrete, which is marked by lateral expansion, it is clear that the lateral or circumferential displacement increases monotonically and, therefore, it can be taken as the most appropriate and sensitive feedback control to obtain the descending branch of the stress-strain diagrams. In the absence of a circumferential extensometer, a special device was designed to measure the lateral deformations, see Fig 1.

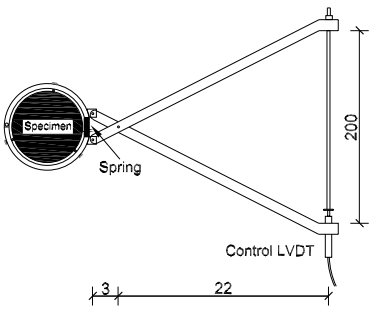

Fig 1 – Device for the lateral displacement control. Measurements in cm.

This device is composed by a central ring that is attached locally to the specimen by means of three steel screws. The expansion of the ring is made possible by the lateral spring. The couple of rods attached to the central ring can move freely when the lateral displacement of the specimen increases, since they are connected through an axis. The control LVDT is placed at the end of one of the rods and is able to measure the deviation between both rods during the compression test. Besides the possibility of testing the specimens by means of the lateral displacement, the device allows the amplification of the actual diametric displacement by a factor of seven, which means that if the programmed velocity of the control LVDT is 2μm/s, the corresponding lateral increment measured in the specimen is approximately 0.3μm/s.

In order to reduce the friction between the specimen and the steel platens, two sheets of Teflon with a thickness of 100μm were placed at the interfaces between the specimen and the steel platens. The axial measurements were carried out by means of three LVDTs (linear field of 20mm with a resolution of 0.05%) located between the lower and upper platens according to the disposition indicated in Fig 2. In order to obtain the Young's modulus, *E*, and the Poisson's ratio, ν, two vertical and two lateral strain gauges were glued to the specimen, placed 180º apart at mid height of three specimens in each series.

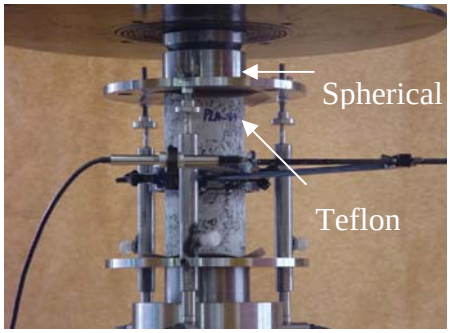

Fig 2 – Test setup.

The test procedure was composed by two phases. In the first phase, so that the lateral LVDT could measure clear horizontal displacements and thus difficulties in the lateral control could be avoided, the specimen was loaded in load control up to a force of 80kN. Subsequently, the control was switched to displacementcontrol by means of the horizontal LVDT at a rate of 2μm/s which corresponds to a rate of the lateral displacementof the specimen of about 0.3μm/s.

3 - RESULTS

3.1 Stress-strain diagrams

The typical stress-lateral strain, stress-axial strain and stress-volumetric strain diagrams that characterize the uniaxial

compressive response of the granites up to peak is shown in Fig 3. These diagrams were obtained from the two vertical and two lateral strains measured by the strain gauges. From the axial strain, ε_a, and lateral strain, ε_l, the volumetric strain, ε_v, which is a measure of the relative volume change in the specimen ($\Delta V/V$), is obtained from the following expression:

$$\varepsilon_v = \varepsilon_a + 2\varepsilon_l \quad [1]$$

In general, from these experimental diagrams it is possible to distinguish the following phases: (a) microcracking and pore closure; (b) linear elastic deformation; (c) crack initiation and stable crack growth; (d) crack damage and unstable crack growth; (e) post-peak behaviour.

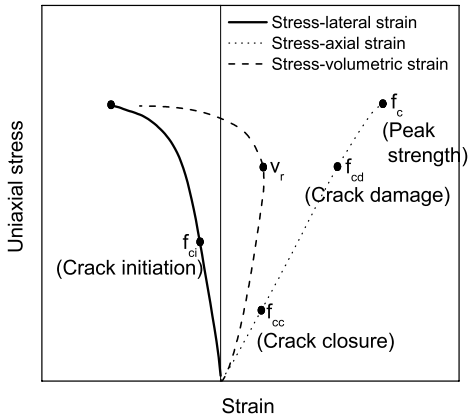

Fig 3 – Typical pre-peak stress-strain diagrams.

Existing microcracking, oriented at an angle to the applied load, and pore closure occurs during the initial stages of loading up to the stress level f_{cc}. This phase is associated to the initial upward concave of the stress-uniaxial strain diagram. After the closure of the pre-existing microcracks, a linear branch of both axial and lateral stress-strain diagrams is observed. The onset of microcraking after the stress level f_{ci} is followed by a nonlinear increase on the lateral and volumetric strains. At this stage, the shape of the stress-axial strain is not sensitive to this mechanism and remains linear. This is the result of the development of the microcracks in axial direction, which are considered by several authors mainly as tensile cracks [Lajtai et al. (1990)]. The unstable microcracking occurs for the crack damage stress level, f_{cd}, and is associated to the point of reversal in the total volumetric strain diagram (V_r). This point is connected to the maximum compaction of the specimen and to the onset of dilation with increase on volume generated by the cracking process. Stress-volumetric and stress-lateral strain diagrams depend on the type of granite. High strength granites exhibit longer initial linear stretch, whereas nonlinear variation on volume is evident at early stages of stress in low strength granites [Vasconcelos (2005)]. After the peak load, the compressive response is characterized by crack localization. At this stage, the tensile or the shear fractures are fully formed and are associated to a significant load carrying capacity decrease. Typical complete axial stress-strain diagrams, obtained by averaging the displaycements recorded by the three LVDTs placed between the steel platens, are displayed in Fig 4.

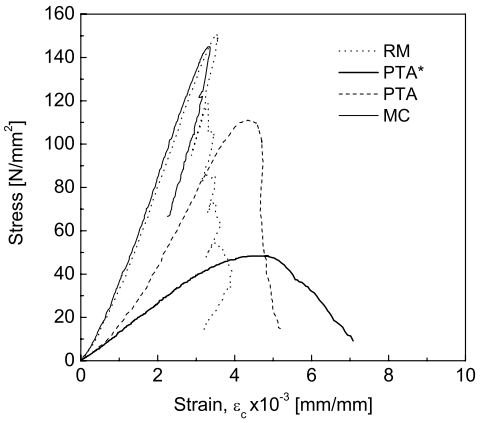

Fig 4 – Typical axial stress-strain diagrams.

It can be observed that the softening branch presents distinct behaviour according to different types of granites. In case of granite PTA and other medium to high strength granites (BA, GA, RM, MC), after localization, the stress-strain diagram drops off abruptly and often it is observed a decrease of the stress and the strain (snap-back behaviour). Another usual feature of the softening diagram for high strength granites consists of the discontinuity characterized by a set of successive abrupt losses (unloading of the material) and recoveries of the loading capacity. In the macrocracking process, the increase of the loading capacity is associated with the

recovery of the stress transfer mechanism between both sides of the macrocrack, which is provided by the grain interlocking. On the contrary, in case of granite PTA* and other low strength granites (MDB, MDB*, PTA*, AF) the shape of the descending branch is smoother, which reflects a softer breakage of internal bonding connections and the preferential shear strain localization. This should involve higher dissipation of energy, when compared to the high strength granites that break in a brittle manner.

3.2 Mechanical properties in the pre-peak regime

The pre-peak behaviour of rocks is essentially characterized by means of the modulus of elasticity, E, and the Poisson's ratio, ν. The modulus of elasticity is calculated by linear fitting of the linear experimental stretch, to which no variation of the first order derivative exists. The Poisson's ratio is calculated from the following expression:

$$\nu = -E/(\text{slope lateral stress/strain diagram}) \quad [2]$$

The values found for the elastic properties exhibit a wide range of variation, see Table 2. The coefficient of variation is indicated inside brackets (%). The minimum (11.1GPa) and the maximum (63.8GPa) values for the modulus of elasticity were obtained for the granites MDB* and MC, respectively. Regarding the Poisson's ratio, the values are in the interval (0.19-0.35) with a mean value of 0.28. The compressive strength also exhibits a large range of variation (26-160 N/mm^2). The values of the coefficient of variation are, in general, quite low for the modulus of elasticity and for the compressive strength. Higher scatter was found for the Poisson's ratio in granites PLA* and MDB*.

For a better understanding of the microcracking process of the granites, the values of the stress markers that indicate the microcracking initiation and the onset of the inelastic deformation (f_{ci}) and the onset of the dilatancy (f_{cd}) were also evaluated, see Table 3. In general, the onset of the microcracking occurs at low stress levels.

Table 2: Mechanical properties of granites.

Granite	f_c (N/mm^2)	E (GPa)	υ
BA	148.5(4.8)	59.9(5.2)	0.29 (2.0)
GA	135.7(5.0)	52.2(2.3)	0.23 (13.1)
GA*	89.5(2.5)	35.8(3.3)	0.30 (17.1)
RM	159.8(2.5)	58.9(1.8)	0.22 (6.5)
MC	146.7(2.8)	63.8(5.6)	0.24 (8.3)
AF⊥fl	66.7(7.8)	15.8(7.2)	0.34 (7.9)
AF//fl	68.9(5.6)	19.0(6.9)	0.31 (17.1)
MDB⊥fl	49.7(5.2)	15.9(13.5)	0.29 (7.4)
MDB//fl	44.8(2.8)	11.6(4.2)	0.31 (3.0)
MDB*⊥fl	35.2(3.4)	11.0(12.0)	0.29 (10.2)
MDB*//fl	26.0(7.1)	12.2(13.6)	0.32 (22.1)
PTA⊥fl	119.1(3.1)	40.5(3.1)	0.21 (21.1)
PTA//fl	109.1(7.3)	41.5(1.6)	0.23 (2.6)
PTA*⊥rp	60.4(4.8)	15.0(7.1)	0.28 (5.8)
PTA*//rp	50.2(11.1)	18.2(3.3)	0.26 (15.4)
PLA⊥rp	147.0(2.6)	53.7(2.8)	0.19 (13.2)
PLA//rp	125.2(6.1)	58.1(2.6)	0.22 (1.1)
PLA*⊥rp	88.5(4.2)	28.9(1.6)	0.32 (13.6)
PLA*//rp	76.9(3.2)	41.6(7.6)	0.35 (30.4)

rp - rift plane
fl – foliation

For low to medium strength granites the values of f_{ci} are lower than $0.3f_c$ and for high strength granites the values lie in the interval $0.3\text{-}0.4f_c$. This finding is, to a large extent, in agreement with the results presented in [Vasconcelos et al. (2008a)] concerning the tensile behaviour of granites, in which a pre-peak inelastic behaviour detected at early stages of loading was pointed out. In fact, the microcracking plays a major role in the compressive behaviour of granites. This is the main reason by which significant increasing values of the Poisson's ratio are recorded during the loading process. The fracture at early loading stages has also been reported for concrete [Choi and Shah (1998)]. For the granites under study, the increase on the microcracking growth is observed also for low levels of crack damage stress, f_{cd}. Only for high strength granites (MC, RM, GA and BA), the values of the crack damage stress are close to the values reported by [Eberhardt et al. (1999)] for Lac du Bonnet granite ($0.7\text{-}0.8f_c$). In

case of low to medium strength granites the onset of dilatancy occurs even for stress levels close but lower than $0.5f_c$ (GA*, AF, MDB, MDB*).

Table 3: Average values of the stress markers.

Granite	f_{ci} (N/mm^2)	f_{cd} (N/mm^2)
BA	55.1 (0.36f_c)	102.2 (0.66 f_c)
GA	50.0 (0.37f_c)	96.2 (0.71 f_c)
GA*	25.1 (0.28f_c)	43.2 (0.49 f_c)
RM	52.4 (0.33f_c)	123.3 (0.78 f_c)
MC	58.5(0.39 f_c)	120.9 (0.81 f_c)
AF⊥fl	17.5(0.26 f_c)	29.1 (0.43 f_c)
AF//fl	15.8(0.23 f_c)	30.1 (0.44 f_c)
MDB⊥fl	14.5(0.30 f_c)	21.8 (0.45 f_c)
MDB//fl	11.8(0.26 f_c)	17.8 (0.40 f_c)
MDB*⊥fl	9.7 (0.27 f_c)	15.2 (0.43 f_c)
MDB*//fl	6.8 (0.27 f_c)	10.7 (0.43 f_c)
PTA⊥fl	30.1 (0.25 f_c)	75.4 (0.63 f_c)
PTA//fl	27.0 (0.24 f_c)	58.3 (0.53 f_c)
PTA*⊥rp	14.1 (0.24 f_c)	31.4 (0.53 f_c)
PTA*//rp	14.7 (0.29 f_c)	26.6 (0.52 f_c)
PLA⊥rp	45.1 (0.31 f_c)	113.3 (0.77 f_c)
PLA//rp	40.8 (0.33 f_c)	85.9 (0.70 f_c)
PLA*⊥rp	26.3 (0.30 f_c)	48.5 (0.55 f_c)
PLA*//rp	19.7 (0.26 f_c)	37.8 (0.49 f_c)

rp - rift plane
fl – foliation

3.3 Fracture energy

As reported by several authors, the compressive loading process of quasi-brittle materials, like rock and concrete, leads to localization of macrocracks when peak stress is attained [Van Mier (1984)]. With respect to the present campaign of compression tests, localization always occurred after peak load is attained, because no signs of perceptible cracking were detected before peak load. Indication of the onset of the localization consists in the detachment of very small particles when decreasing of load carrying capacity is recorded. Examples of failure patterns that illustrate strain localization are displayed in Fig 5.

Although some spread splitting vertical cracks are visible in most specimens, a clear macrocrack localized in a generalized shear band is often present.

Fig 5 - Examples of failed specimens.

In order to take into account the localization and the consequent unloading of the undamaged continuum, the inelastic displacement is calculated by subtraction of the inelastic pre-peak displacement to the total displacement. The stress ratio f/f_c up to which the softening diagram is considered was fixed in 0.33 [Jansen and Shah (1997)]. The procedure to calculate the pre- and post-peak fracture energies, G_{cpre} and G_{cpost}, is indicated in Fig 6.

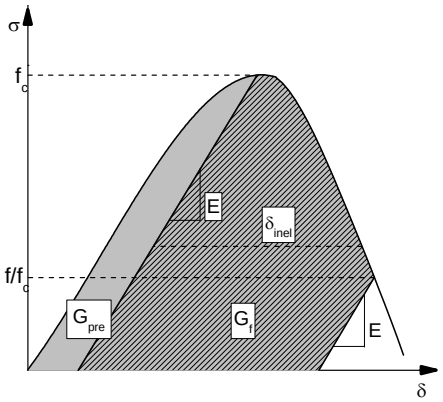

Fig 6 - Procedure used for determination of the pre- and post-peak fracture energies and definition of inelastic displacement, δ_{inel}.

The pre-peak fracture energy corresponds to the amount of energy dissipated during the microcracking process before the maximum load is attained. The mean values of the pre- and post-peak fracture energies are shown in Table 4. The corresponding coefficient of variation is also indicated inside brackets (%). It is observed that moderate values of the coefficient of variation were found. This underlines the reliability of these variables in the fracture characterization in compression. Both values of pre- and post-peak fracture energies depend largely on the type of granite and, therefore, exhibit large range of

variation. The values of pre-peak energy lie in the interval (3.2-10.4N/mm), whereas the values of the dissipated energy in the macroscopic fracture are between 11.8N/mm for granite MDB* and 49.1N/mm for granite PTA*. In addition, the values of the normalized fracture energy are between 0.224mm and 0.874mm for high and low strength granite respectively [Vasconcelos (2005)].

Table 4: Mean values of the fracture energy.

Granite	G_{cpre} (N/mm)	G_{cpost} (N/mm)
BA	7.1 (21.1)	45.3 (8.3)
GA	7.9 (15.6)	43.3 (8.2)
GA*	8.5 (26.0)	31.3 (8.2)
RM	5.1 (20.6)	42.1 (14.4)
MC	3.7 (33.4)	39.6 (4.6)
AF⊥fl	10.4 (9.6)	47.8 (9.5)
AF//fl	8.2 (11.0)	37.3 (9.3)
MDB⊥fl	6.9 (9.4)	22.3 (23.4)
MDB//fl	8.3 (15.2)	30.3 (8.2)
MDB*⊥fl	4.6 (15.0)	17.2 (8.0)
MDB*//fl	3.2 (10.1)	11.8 (14.0)
PTA⊥fl	8.1 (28.1)	45.5 (6.1)
PTA//fl	7.1 (16.4)	44.4 (24.6)
PTA*⊥rp	11.8 (9.2)	49.1 (3.2)
PTA*//rp	7.3 (17.4)	28.0 (17.5)
PLA⊥rp	8.0 (16.8)	31.7 (20.7)
PLA//rp	4.2 (22.9)	32.8 (10.0)
PLA*⊥rp	7.4 (5.3)	35.7 (2.8)
PLA*//rp	4.6 (26.4)	24.2 (15.6)

4 – INFLUENCE OF MICROSTRUCTURAL FACTORS ON THE COMPRESSIVE BEHAVIOUR

4.1 Internal structure

From a comparative analysis of the shape of the complete stress-strain diagrams and a quantitative comparative analysis of the elastic and fracture properties, a dependence of the compressive behaviour on the direction of the applied load is detected. From Fig 7, it can be seen that granite PLA exhibits higher compressive strength in the direction perpendicular to the planar anisotropy. This is also valid to granite PTA. This fact can be explained by the influence of internal structure (related with the preferential alignment of minerals) on the fracture process under uniaxial unconfined compression. In the compressive fracture process of these granites the mode I cracking is the predominant fracture mechanism, which is largely confirmed by the parallel or subparallel direction of the main macrocrack relatively to the applied load. The same case occurs in the direct tensile tests when the applied load is in the direction perpendicular to the rift or foliation planes [Vasconcelos et al. (2007)]. Similar results were found in granites PTA*, MDB and MDB*, where the compressive strength presents higher value for loading acting in the direction perpendicular to the rift plane and to the foliation plane.

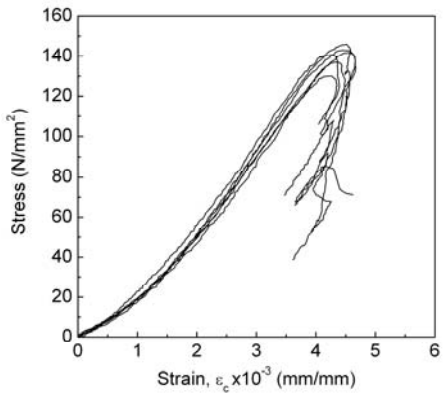

(a)

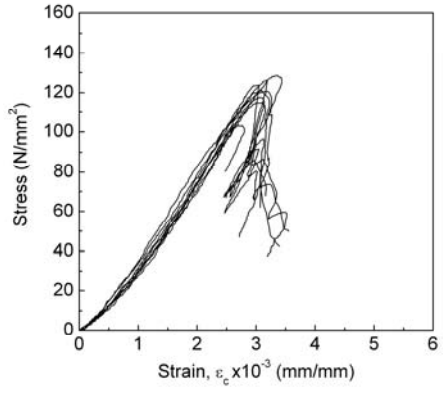

(b)

Fig 7 - Stress-strain diagrams for granite PLA in compression; (a) direction perpendicular to the rift plane; (b) direction parallel to the rift plane.

With respect to the elastic properties, in general, the granites exhibit higher axial stiffness in the directions parallel to the rift

or to the foliation planes. This seems to indicate that both oriented feldspar phenocrystals and biotite increase the stiffness of the material. This assumption is also confirmed by the lower values of Poisson's ratio in granites PLA, PLA*, PTA and PTA* in the direction perpendicular to the rift or foliation planes. The analysis of the ascending branch of the stress-strain diagrams for the granites PLA, PLA* and PTA, indicates that the extent of the initial upward concave is more pronounced when the granite is loaded in the perpendicular direction to the rift or foliation planes. The crack closure process is, therefore, more significant when the planar anisotropy is oriented in the perpendicular direction to the applied load. This anisotropic behaviour appears thus to be the result of a larger amount of pre-existing open microcraks oriented preferentially according to the foliation or the rift plane. At this stage, the compressive behaviour is not only affected by the solid skeleton but also by the open microcracks [Vasconcelos et al. (2008b)]. The anisotropy is also relevant when the stress markers are analysed, particularly in case of the crack damage stress, f_{cd}. In granites PLA, PLA*, PTA and PTA*, the values of the crack damage stress exhibit higher levels and simultaneously higher values of volume decrease in the direction perpendicular to the planar anisotropy. With respect to the deformation, if the maximum compaction is subtracted by the value of variation of volume corresponding to the onset of the microcracking, it is found that microcracking involves higher decrease in volume in the direction perpendicular to the rift or foliation planes [Vasconcelos (2005)].

4.2 Weathering state

The shape of the stress-strain diagrams shows also clearly that significant distinct pre- and post-peak compressive behaviour is addressed for fresh and weathered granites. Besides the higher values of the compressive strength, the slope of the ascending branch of the stress-strain diagrams is considerably higher in fresh granites, in comparison with the slope exhibited by weathered granites, see Fig 8. The deformation capacity until peak load is significantly larger in weathered granites. Fresh granites exhibit very brittle response, associated to a steep and often discontinuous softening branch, whereas for weathered granites the descending branch is mostly continuous and smooth. The remarkable difference of the post-peak behaviour seems to be the result of a distinct mechanism of macrocracking localization.

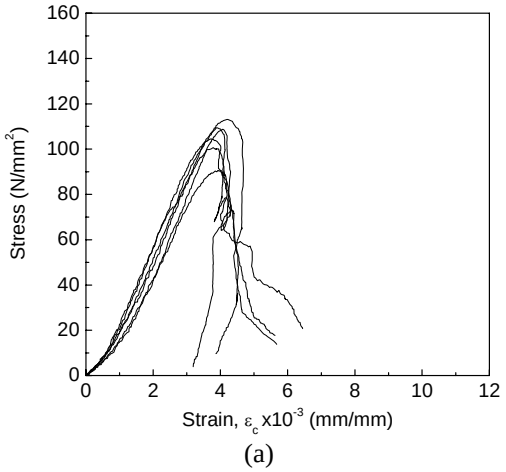

Fig 8 – Stress strain diagrams; (a) granite PTA in the direction parallel to the foliation plane; (b) granite PTA* in the direction parallel to the foliation plane.

In effect, in fresh granites the main macrocrack that results from the localization is parallel or sub-parallel to the axial load. In weathered granites the localization occurs predominantly in a shear band. The ultimate deformation is considerable higher in weathered granites, which appears as an outcome of a more ductile behaviour of the material. By

comparing the mean values of the elastic properties that characterize the pre-peak behaviour of the granites, modulus of elasticity, E, and Poisson's ratio, ν, it is clear that much higher values of the modulus of elasticity are associated to fresh granites and there is a trend for the Poisson's ratio to increase with weathering state. The decrease in the compressive strength for weathered granites reaches considerable values, ranging between 47.6% and 54.0% of the less weathered strength, respectively for granites MDB* (direction perpendicular to foliation) and PTA* (direction parallel to foliation). Note also the remarkable lowering of the compressive strength of granites MDB and MDB*, with high porosity. As discussed in [Vasconcelos (2005)], both the compressive strength and modulus of elasticity decreases considerably with the increase on the porosity, which increases with the weathering of the granites.

The onset of microcracking was found to occur earlier for weathered granites, being the difference more significant for granites GA, PLA and PTA in the direction perpendicular to the foliation. A similar trend was observed for the crack damage stress, with dilatancy taking place for remarkably higher stress levels in case of fresh granites. In weathered granites, the propagation and interaction of microcracking occurs for low stresses, roughly at $0.5f_c$. In granites GA*, MDB and MDB* the stress levels found for f_{cd} are even lower than $0.5f_c$.

4.3 Moisture content

In order to obtain a better insight on the influence of water saturation on the compressive behaviour of granites, twenty-five compression tests were performed on six types of granites. From the axial stress-strain diagrams, it is possible to obtain the compressive mechanical properties, namely strength, stiffness and fracture energy, for comparison with the values obtained in dry conditions. The qualitative analysis of the complete stress-strain diagrams obtained for dry and saturated specimens is shown in Fig 9. This indicates that a significant decrease on the compressive strength is recorded in saturated specimens, with respect to dry specimens. Furthermore, under saturated conditions the material exhibits lower deformation capacity at peak load and at the end of the test. However, the saturated specimens show a slightly smoother descending branch than dry specimens. In spite of lower amount of specimens tested under saturated conditions, the complete stress-stain diagrams exhibit lower scatter both in the pre- and post-peak regimes.

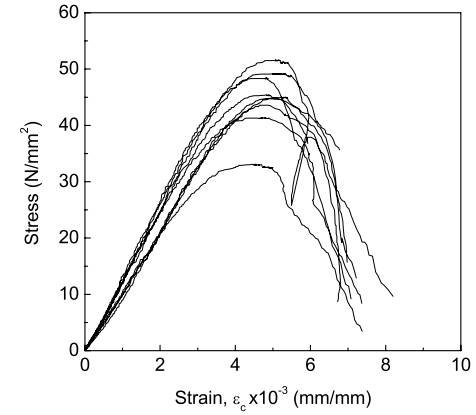

(a)

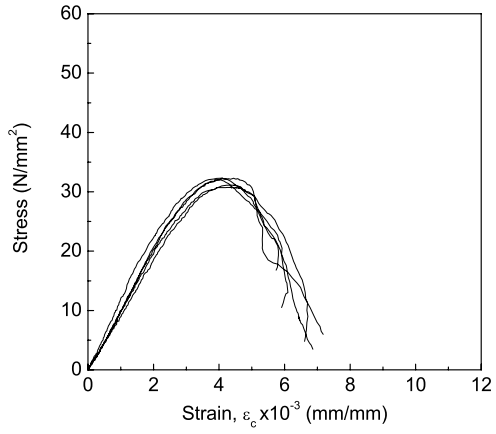

(b)

Fig 9 - Axial stress-strain diagrams for granite PTA*; (a) dry conditions; (b) saturated conditions.

The wet specimens undergo a reduction in strength ranging from 27.0% to 42.3%. Similar decreasing trend was recorded in the axial stiffness that exhibits differences between 16 and 36%. These results are in agreement with others reported in literature [Gupta and Rao (2000)]. Hawkins (1998) reported losses in compressive strength ranging between 8% and 59%. The lower stiffness and strength in saturated

specimens can be explained by the changing of stone skeleton due to water filling of pores and voids, as the water pressure acts on the existing pores and microcracks, leading to earlier fracture. The fracture energy involved in the pre-peak microcracking in saturated conditions is always lower than in dry conditions. The post-peak fracture energy exhibits also lower values in saturated specimens

5 - CONCLUSIONS

In order to characterize the uniaxial compressive behaviour of a masonry stone (granite), a campaign of uniaxial tests was carried out at University of Minho by using the circumferential displacement feedback control, enabling the obtaining of the complete stress-strain diagrams, from which elastic and fracture properties were derived. It was observed that the variation on the mechanical and fracture properties has been explained by microstructural aspects such as the internal texture and weathering state. In particular, it was found that the rock easiest splitting plane (rift plane) and the foliation plane are sources of anisotropy concerning the compressive parameters. Both the pre- and post-peak compressive behaviour are highly affected by the weathering state of granites and moisture content. The compressive strength, as well as the modulus of elasticity undergoes remarkable decrease in weathered granites, while the Poisson's ratio presents higher values. This behaviour reflects the structural alterations associated to increase of porosity.

REFERENCES

ASTM D2938-95 – Standard Test Method for Compressive Strength and Elastic Moduli of Intact Rock Core Specimens under Varying States of Stress and Temperatures, American Society for Testing Materials, 2002.

Carpinteri, A., Scavia, C., Yang, G.P., Microcrack propagation, coalescence and size effects in compression; Engineering Fracture Mechanics, 54(3), 335-347, 1996.

Choi, S., Shah, S.P., Fracture mechanism in cement-based materials subjected to compression, Journal of Engineering Mechanics, 124(1), 94-102, 1998.

Eberhardt, E., Stimpson, B., Stead, D., Effects of grain size on the initiation and propagation thresholds of stress-induced brittle fractures, Rock Mechanics and Rock Engineering, 32(2): 81-99, 1999.

Griffith, A.A., The phenomena of rupture and flow in solids. Philos. Trans. Roy. Soc. London, series A, 221, 163-198, 1920.

Gupta, A.S., Rao, K.S., Weathering effects on the strength and deformational behaviour of crystalline rocks under uniaxial compression state, Engineering Geology, 56, 257-2574, 2000.

Hawkins, A.B., Aspects of rock strength, Bulletin of Engineering Geology and Environment, 57, 17-30, 1998.

Hudson, J.A., Harrison, J.P. H., Engineering rock mechanics, an introduction to the principles, 1st edition, Pergamon, 1998.

ISRM Suggested Methods. 1981. Suggested method for determining uniaxial compressive strength and deformability of rock materials, In: Brown E.T., ISRM Suggested Methods. Pergamon, Oxford.

Jansen, D.C., Shah, S.P., Rossow, E.C., Stress-strain results of concrete from circumferential strain feedback control testing, ACI Materials Journal, 92 (4), 419-428, 1995.

Lajtai, E. Z., Carter, B.J., Ayari, M.L., Criteria for brittle fracture in compression, Engineering Fracture Mechanics, 37(1), 59-74, 1990.

Van Mier, J.B., Strain-softening of Concrete under Multiaxial Loading Conditions, PhD Thesis, Eindhoven, University of Technology, The Netherlands, 1984.

Vasconcelos, G., Experimental investigations on the mechanics of stone masonry: characterization of granites and behaviour of stone masonry shear walls, PhD thesis, University of Minho, Portugal, 2005.

Vasconcelos, G. Lourenço, P.B., Alves, C.A.S., Pamplona, J., Analysis of the weathering and internal structure on the engineering properties of granites, ISRM, International Workshop W3 – Preservation of natural stone and rock weathering, Estaire&Ollala eds, Mérida, Spain, 75-84, 2007.

Vasconcelos, G. Lourenço, P.B., Alves, C.A.S., Pamplona, J., Experimental characterization

of the tensile behaviour of granites, International Journal of Rock Mechanics and Mining Sciences, 45(2), 268-277, 2008a.

Vasconcelos, G. Lourenço, P.B., Alves, C.A.S., Pamplona, J., "Ultrasonic evaluation of the physical and mechanical properties of granites", Ultrasonics, 48(5), 453-466, 2008b.

Vonk, R.A., A micromechanical investigation of softening of concrete loaded in compression, volume 38, nº3 Heron, pp.94, 1993.